Geomechanics and Engineering, *Vol. 21, No. 3 (2020) 279-288*
DOI: https://doi.org/10.12989/gae.2020.21.3.279

Jet-grouting in ground improvement and rotary grouting pile installation: Theoretical analysis

You Wang[1a], Lin Li*[2], Jingpei Li[1b] and De'an Sun[3c]

[1]*Department of Civil Engineering, Tongji University, Shanghai 200092, China*
[2]*Department of Civil and Environmental Engineering, Louisiana State University, LA 70803, U.S.A.*
[3]*Department of Civil Engineering, Shanghai University, Shanghai 200444, China*

(Received October 22, 2019, Revised February 16, 2020, Accepted March 23, 2020)

Abstract. The permeation grouting is a commonly used technique to improve the engineering geology condition of the soft ground. It is of great significance to predict the permeation range of the grout so as to ensure the effects of grouting. This paper conducts a theoretical analysis of jet-grouting effects in ground improvement and rotary grouting pile installation by utilizing deformation-permeation coupled poroelastic solutions based on Biot's theory and Laplace-Fourier integral transform technique. The exponential function and the intermittent trigonometric function are chosen to represent time-dependent grouting pressure usually encountered in ground improvement and rotary grouting pile installation process, respectively. The results, including the radial displacement, the hoop stress, the excess pore fluid pressure, the radial discharge, and the permeation radius of grout, are presented for different grouting time, radial positions and grouting lengths. Parametric study is conducted to explore the effects of variation of the exponent in the exponential grouting pressure-time relationship on grouting-induced responses. It is expected that the proposed solutions can be used to estimate the permeation range of grouting in ground improvement and rotary grouting pile installation.

Keywords: poroelastic; coupled permeation and deformation; ground improvement; rotary grouting pile; grouting pressure

1. Introduction

Since the soft ground usually shows low bearing capacity and high compressibility, it will exhibit substantial ground subsidence under vertical loads and further cause failure of engineering structures. Hence, ground improvement through grouting is needed to avoid such geological hazards (Bergado *et al.* 1996, Shehata and Poulos 2018, Singh 2018). Jet-grouting is a commonly utilized technique to harden the ground or reinforce rock masses and form rotary grouting piles in practical engineering by filling voids and replacing pore fluid with grouts in soil (Lignola *et al.* 2008, Zhang *et al.* 2015, Chang *et al.* 2016, Kim and Park 2017, Shen *et al.* 2017, Njock *et al.* 2018, Zhang *et al.* 2018, Celik 2019, Sun *et al.* 2019, Zou and Zhang 2019). The injected grout solidifies and produces a cemented soil body, which would greatly enhance the bearing capacity of the soft ground. Since the area of cemented soil body primarily depends on the permeation range, it is of great significance to determine the permeation range of the grout so as to estimate the grouting effects in practice.

Over the past few decades, a variety of theoretical models have been developed to investigate the diffusion process of grouts in the soil. These theoretical solutions can be broadly divided into rheology solution, Biot's coupled solution and cavity expansion solution. Based on the rheology equation, Wallner (1976) modeled the grouts as Bingham fluids to investigate permeation of cement pastes in jointed rocks. Hassler *et al.* (1992) also presented an analytical model, which assumes the grout as Newtonian or Bingham fluids, to describe diffusion of grout in jointed rock. Yang *et al.* (2004) presented a spherical permeation model to formulate the permeation radius of Bingham fluids injected into sandy soils and predicted the grouting pressure needed along the depth. Extensive research efforts, which take more properties of grout into account, have been devoted to analyzing diffusion of grouting fluids in soils. Yang *et al.* (2011) investigated column-hemispherical penetration mechanisms considering time-dependent viscosity of grout. Experiments were conducted to verify the solutions, the observations of which showed good agreement with the theoretical results. More recently, Hou *et al.* (2019) considered the variation of the viscosity of grout with time and proposed an improved model for both cylindrical and spherical permeation of Bingham fluids in porous media. However, the permeation mechanisms for Bingham or Newtonian fluids, based on the rheology equation, only take the diffusion of grouts into account,

*Corresponding author, Ph.D.
E-mail: 1310230@tongji.edu.cn
[a]M.Sc. Student
E-mail: 1832366@tongji.edu.cn
[b]Professor
E-mail: lijp2773@tongji.edu.cn
[c]Professor
E-mail: sundean@shu.edu.cn

ISSN: 2005-307X (Print), 2092-6219 (Online)

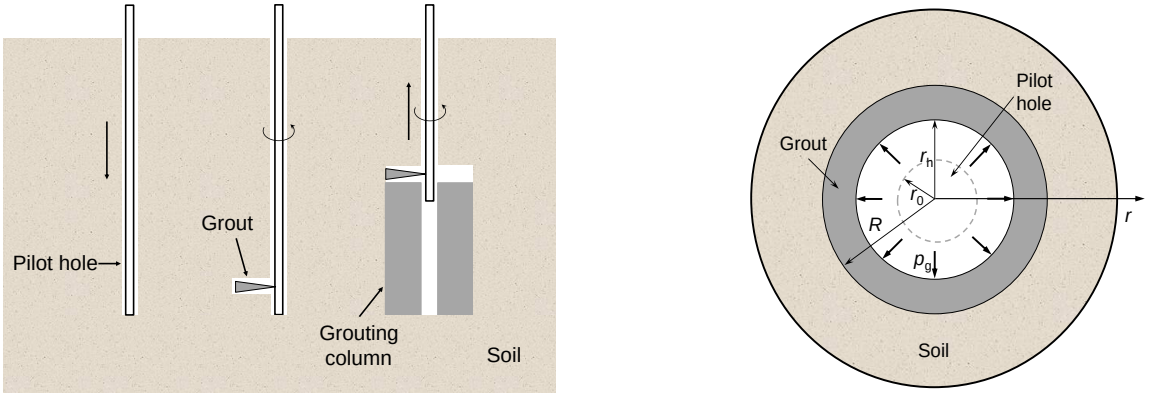

Fig. 1 Scheme of jet-grouting process

while neglect the quasi-static deformation of soils. The poroelasticity theory proposed by Biot (1941), which well couples the volumetric changes of soil and the permeation behaviors of grouting fluids, has great potential in modelling the permeation range of grout for ground improvement and rotary grouting pile installation (Detournay and Cheng 1988, Abousleiman and Cui 1998, Mehrabian and Abousleiman 2013, Song *et al.* 2019). Based on Biot's theory, Rajapakse (1993) developed an analytical solution for grouts injection in a borehole, but the solution is only applicable to the case where constant uniform radial traction is applied to the borehole wall. As for the cavity expansion model, Liu *et al.* (2017) proposed a cavity expansion model to estimate the installation effects of high pressure jet-grouting columns. The spherical cavity expansion theory is adopted to derive the approximate solutions in semi-infinite soils, which are compared with both the numerical results acquired from FEM and other well-documented solutions. Zou and Zuo (2017) idealized the synchronous grouting process of shield tunnel as cylindrical cavity expansion and proposed a theoretical solution for synchronous grouting of shield tunnel under non-axisymmetric displacement boundary. Li *et al.* (2019) also developed a theoretical model based on the cavity expansion theory to determine the limiting grouting pressure for compaction grouting. However, these cavity expansion theory-based models fail to take the permeation of grout into account. It can be found that the previous theoretical models pertaining to grouting mechanisms either neglect the volumetric changes of soils or ignore the permeation of the grout in the soil mass. A poroelastic solution, which properly considers the real time-dependent grouting pressure, has seldom been covered in the published literature.

This paper aims at developing an analytical model to investigate the jet-grouting effects by adopting Biot's poroelasticity theory, in which the volumetric change of soil couples the permeation of grout. Two typical time-dependent boundary conditions are considered in this study to simulate the real grouting pressure-time relationships encountered in ground improvement and rotary grouting pile installation. Boundary condition I represents the intermittent grouting when forming rotary grouting piles due to rotation of the grouting pipe. Boundary condition II corresponds to the grouting process in ground improvement without rotation of the grouting pipe. Parametric studies are conducted to explore the impacts of the exponent in boundary condition II on different grouting-induced responses. It is expected that the proposed theoretical model could better explain the coupling mechanism between deformation of soil and permeation of grouting fluids and provide guidelines for design and construction of grouting.

2. Background and theoretical model of jet-grouting

The soft ground may experience great settlement under the load transferred from the superstructures constructed over it (Cai *et al.* 2006). In such situations, jet-grouting is an effective way to improve the strength and stiffness of the ground so as to reduce the ground settlement. Also, deep foundations, such as the rotary grouting pile, are necessary if grouting in surface layer is unable to sustain the superstructures. (Jalili and Shabani 2019). According to the grouting procedure, the jet-grouting process in ground improvement and rotary grouting pile installation can be approximately modeled as the expansion of the borehole and the permeation of grouts into surrounding soils under the grouting pressure, as shown in Fig. 1. As seen in the figure, the grouting pipe is first penetrated into the borehole with an initial radius of r_0. Then, the grouting pipe is rotated and risen up to inject the grout into the surrounding soil. During the grouting process, the borehole gradually expands from the initial radius r_0 to the ultimate radius r_h accompanied by permeation of the grouting fluids in the porous media. The actual boundary conditions are generally extremely complicated during the jet-grouting process, attributed to many factors such as the grouting rate, components of the injected fluids, jet propagation across the space included between nozzles and the intact soil and so on (Modoni *et al.* 2006). For simplicity, the injected fluids are regarded as the single fluid system, which contain grout only without air and water. It is also assumed that the jet-grouting process in semi-infinite soil is an axisymmetric problem with uniform grouting pressure being applied to the borehole wall. Three types of grouting techniques are widely covered in grouting engineering: the permeation grouting method, the fracturing grouting method, and the compaction grouting method. In this study, the first kind of grouting mechanism is chosen to investigate the jet-

grouting process. Based on Biot's theory, the problem considered can be reduced to solving a partial differential equation group, which couples volumetric changes of soil and the permeation of grout.

3. General solutions

In this study, the poroelasticity theory proposed by Biot (1941) is adopted to illustrate the coupled deformation-permeation mechanism of jet-grouting in the porous media. In terms of the axial symmetry, the problem considered can be formulated by three basic governing equations, which are expressed with respect to the cylindrical coordinate system as follows

$$\left(\nabla^2-\frac{1}{r^2}\right)w_r+\frac{1}{1-2\nu}\frac{\partial\varepsilon_v}{\partial r}+\frac{1}{G}\frac{\partial p}{\partial r}=0 \tag{1}$$

$$\nabla^2 w_z+\frac{1}{1-2\nu}\frac{\partial\varepsilon_v}{\partial z}+\frac{1}{G}\frac{\partial p}{\partial z}=0 \tag{2}$$

$$\frac{2Gk(1-\nu)}{1-2\nu}\nabla^2\varepsilon_v=\frac{\partial\varepsilon_v}{\partial t} \tag{3}$$

where w_r and w_z represent the displacement in *r*- and *z*-directions, respectively; p is the excess pore fluid pressure; ε_{v} denotes the volumetric strain of soils; G and k, are denoted as the shear modulus and the permeability coefficient of the porous medium; ν represents Poisson's ratio of soil; ∇^2 is referred to as the Laplace operator and is expressed as

$$\nabla^2=\frac{\partial^2}{\partial r^2}+\frac{1}{r}\frac{\partial}{\partial r}+\frac{\partial^2}{\partial z^2} \tag{4}$$

According to generalized Hooke's law, the stress-strain relationship can be given in the tensor form as follows

$$\sigma_{ij}=2G\left[\varepsilon_{ij}+\frac{\nu}{1-2\nu}\varepsilon_{kk}\delta_{ij}\right]+p\delta_{ij} \tag{5}$$

where δ_{ij} is Kronecker's delta symbol; σ_{ij} and ε_{ij} represent the stress and strain tensors, respectively. It should be noted that uniform radial grouting pressures are imposed on the borehole wall during the installation process of rotary grouting piles, and thus the circumferential displacement (w_θ), the shear stresses ($\sigma_{r\theta}$ and $\sigma_{z\theta}$) and shear strains ($\varepsilon_{r\theta}$ and $\varepsilon_{z\theta}$) all vanish because of the axisymmetric geometry and loading conditions.

Another noteworthy point is that Eq. (3) can be simplified if the variables are non-dimensionalized by taking the cavity radius r_{h} as a unit length and $r_{\mathrm{h}}^2(1-2\nu)/[(2Gk(1-\nu)]$ as a unit of time. The dimensionless quantities will yield dimensionless solutions, which is representational while displaying the final results in this study.

To solve the partial differential equations above, the Laplace-Fourier integral transform technique is employed, and therefore the two transforms of a function are first introduced here. The Laplace transform of a function $f(r,z,t)$ with respect to time t, denoted as $\bar{f}(r,z,s)$, can be expressed as

$$\bar{f}(r,z,s)=\int_0^{+\infty}f(r,z,t)e^{-st}dt \tag{6}$$

Correspondingly, the inverse transform is cast as follows

$$f(r,z,t)=\int_{\gamma-i\infty}^{\gamma+i\infty}\bar{f}(r,z,s)e^{st}ds \tag{7}$$

where s represents the Laplace transform parameter; Re $s=\gamma$, is a line on s plane, which is to the right of all singularities of $\bar{f}$; and i denotes the imaginary unit.

As for the Fourier transform, it is not hard to give the following transform formula of the function $\bar{f}$ above.

$$f^*(r,\omega,s)=\frac{1}{2\pi}\int_{-\infty}^{+\infty}\bar{f}(r,z,s)e^{i\omega z}dz \tag{8}$$

where f^* is the Fourier transform of $\bar{f}$; ω represents the Fourier transform parameter.

Inversely, $\bar{f}$ can be expressed with an integral as follows.

$$\bar{f}(r,z,s)=\frac{1}{2\pi}\int_{-\infty}^{+\infty}f^*(r,\omega,s)e^{-i\omega z}d\omega \tag{9}$$

It is convenient to convert Eq. (3) to the following form by non-dimensionalizing all the quantities, as has been demonstrated previously.

$$\nabla^2\varepsilon_v=\frac{\partial\varepsilon_v}{\partial t} \tag{10}$$

The solution can be obtained as follows by applying the Laplace-Fourier transform to variables t and z.

$$\varepsilon_v^*=C_1(\omega)K_0(Ar)+C_2(\omega)I_0(Ar) \tag{11}$$

where I_0 and K_0 are denoted as modified Bessel functions of the first and second kind, respectively; $C_1(\omega)$ and $C_2(\omega)$ are two arbitrary functions with respect to the variable ω; A is an intermediate variable and can be expressed with ω and s as $\sqrt{\omega^2+s}$.

It is interesting to note that the value of the function I_0 will grow to infinity as the radial distance r increases. However, it is recognized that the volumetric strain remains finite everywhere in the porous medium, which demands C_2 to be zero. Therefore, the expression of ε_v^* can be simplified as follows

$$\varepsilon_v^*=C_1(\omega)K_0(Ar) \tag{12}$$

Through proper differentiation of Eqs. (1) and (2), the excess pore fluid pressure, p, is correlated with the volumetric strain in the following form.

$$\nabla^2 p=-2G\frac{1-\nu}{1-2\nu}\nabla^2\varepsilon_v \tag{13}$$

Similarly, Eq. (13) can be solved by applying the two transforms and substituting Eq. (12) into Eq. (13), the result of which is shown below.

$$p^*=2G[C_3|\omega|K_0(|\omega|r)-\frac{1-\nu}{1-2\nu}C_1K_0(Ar)] \tag{14}$$

where C_3 is an arbitrary function of ω.

After deriving expressions of the volumetric stain and the excess pore fluid pressure, the displacement in z-direction, w_z, is obtained by substituting Eqs. (12) and (14) into Eq. (2).

$$w_z^* = C_4|\omega|K_0(|\omega|r) + i\omega rC_3K_1(|\omega|r) + \frac{i\omega C_1}{s}K_0(Ar) \quad (15)$$

where C_4 is also an arbitrary function with respect to ω.

Making use of Eq. (1) and the stress-strain relationship, it is not difficult to express the radial displacement w_r^*, radial stress σ_{rr}^*, circumferential stress $\sigma_{\theta\theta}^*$ and shear stress σ_{rz}^* as follows

$$w_r^* = -\frac{C_1A}{s}K_1(Ar) - C_3|\omega|rK_2(|\omega|r) + i\omega C_4K_1(|\omega|r) \quad (16)$$

$$\sigma_{rr}^* = 2G\{C_1\left[\frac{\omega^2}{s}K_0(Ar) + \frac{A}{sr}K_1(Ar)\right] + C_3|\omega|[K_2(|\omega|r) + K_0(|\omega|r) + |\omega|rK_1(|\omega|r)] - i\omega C_4[|\omega|K_0(|\omega|r) + \frac{K_1(|\omega|r)}{r}]\} \quad (17)$$

$$\sigma_{\theta\theta}^* = 2G\{-C_1\left[\frac{A}{sr}K_1(Ar) + K_0(Ar)\right] - C_3|\omega|[K_2(|\omega|r) - K_0(|\omega|r)] + \frac{i\omega}{r}C_4K_1(|\omega|r)\} \quad (18)$$

$$\sigma_{rz}^* = 2G\{-iC_1\frac{\omega A}{s}K_1(Ar) + iC_3\omega[K_1(|\omega|r) - |\omega|rK_2(|\omega|r)] - \omega^2C_4K_1(|\omega|r)\} \quad (19)$$

The solutions obtained above are the Laplace-Fourier transforms of the original functions, and thus the final results should be presented with the inverse formula.

Since the permeation of grout in the porous medium conforms to Darcy's law, the radial fluid discharge, q_r, can be expressed with the following equation.

$$q_r = k\frac{\partial p}{\partial r} \quad (20)$$

However, there has been unified cognition that the complexity of the integral in the inverse transform formula tends to make it impossible to obtain a rigorous analytical solution of the quantities above. Thus, some numerical methods have been proposed to tackle the infinite integral, a well-known method of which is reported in Stehfest's paper (1970) as follows

$$f(t) = \frac{1n2}{t}\sum_{k=1}^{N} a_k\bar{f}(\frac{kln2}{t}) \quad (21)$$

where $\bar{f}$ is the Laplace transform of f; N is an even integer which is taken as a number larger than 8 to achieve satisfactory accuracy; a_k, however, is determined with the following equation

$$a_k = (-1)^{k+N/2}\sum_{i=\lfloor\frac{k+1}{2}\rfloor}^{\min(k,\frac{N}{2})}\frac{i^{\frac{N}{2}}(2i)!}{\left(\frac{N}{2}-i\right)!\,(i-1)!\,(k-i)!\,(2i-k)!\,i!} \quad (22)$$

The Fourier inversion can be directly conducted with simple numerical integral methods for the reason that only the points at $z = 0$ are considered during the whole analysis and thus the integrand of the inverse formula is reduced to a real function of ω without the imaginary unit.

4. Time-dependent boundary conditions

The borehole wall is assumed to be subjected to uniform grouting pressure over a segment of length $2b$. Two kinds of time-dependent boundary conditions are selected in this study to represent the grouting pressures encountered in ground improvement and rotary grouting pile installation, as shown in Fig. 2. It should be noted that a fully permeable surface is applied to the boundary. Corresponding solutions are obtained by solving the boundary-value problems in the following.

4.1 Exponential grouting pressure-time relationship

A simple grouting pressure-time relationship is described with the exponential function, which is commonly encountered in ground improvement. The boundary condition can be expressed with the dimensionless variables as

$$\sigma_{rr}(1,\tilde{z},\tau) = f_u(1-e^{-B\tau})[(H(\tilde{z}+\tilde{b}) - H(\tilde{z}-\tilde{b})] \quad (23)$$

where $\tilde{z}$, τ and $\tilde{b}$ are non-dimensionalized variables; f_u represents the limit value of grouting pressure; B is the

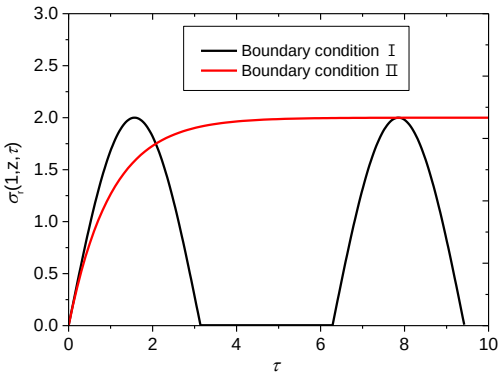

Fig. 2 Two kinds of time-dependent boundary conditions

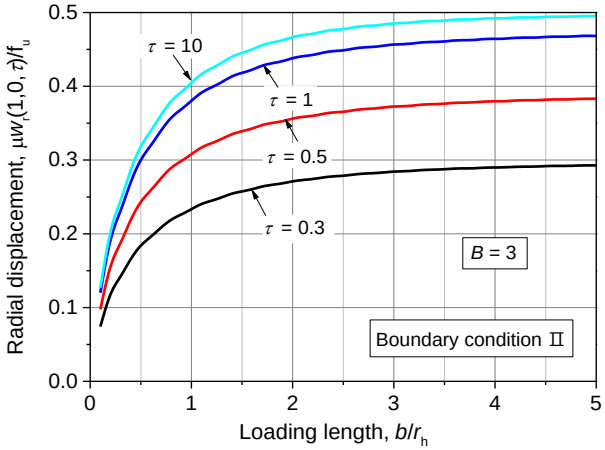

Fig. 3 Variation of radial displacement at borehole wall ($z = 0$) with loading length for different grouting time under boundary condition II

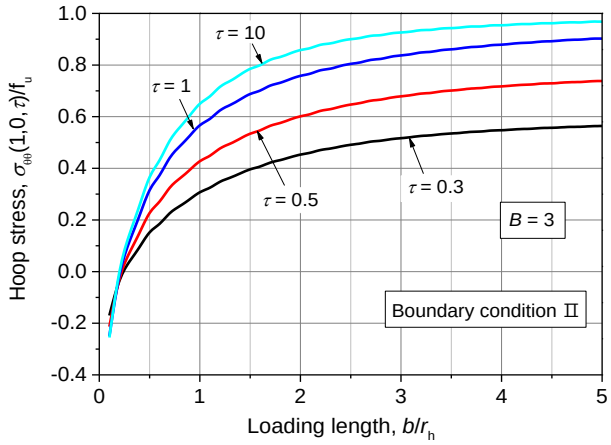

Fig. 4 Variation of hoop stress at borehole wall ($z = 0$) with loading length for different grouting time under boundary condition II

exponent in the grouting pressure-time relationship; $H()$ is denoted as the Heaviside step function.

To solve the boundary-value problem mentioned above, the Laplace-Fourier transform needs to be applied to Eq. (23) to obtain the boundary condition in the following form.

$$\sigma_{rr}^*(1,\omega,s) = -2\frac{1+e^{-2\pi}}{1-e^{-2\pi}}\frac{1}{1+s^2}\frac{\sin(\omega\tilde{b})}{\omega} = p_g^* \quad (24)$$

Other boundary conditions for the fully permeable surface can be easily expressed with the following two equations

$$p^*(1,\omega,s) = 0 \quad (25)$$

$$\sigma_{rz}^*(1,\omega,s) = 0 \quad (26)$$

Using Eq. (14), the excess pore fluid pressure given by Eq. (25) is reduced to the following relationship between C_1 and C_3.

$$C_1 = \frac{(1-2\nu)|\omega|K_0(|\omega|)}{(1-\nu)K_0(A)}C_3 = DC_3 \quad (27)$$

where D is an intermediate coefficient expressed as $[(1-2\nu)|\omega|K_0(|\omega|)]/(1-\nu)K_0(A)$.

The rest of the coefficients can be determined by substituting Eqs. (17), (19) and (27) into Eqs. (24) and (26), expressions of which are cast below.

$$C_3 = -\frac{b_1}{2GM}p_g^* \quad (28)$$

$$C_4 = \frac{b_2}{2GM}p_g^* \quad (29)$$

where

$$b_1 = -\omega^2 K_1(|\omega|) \quad (30)$$

$$b_2 = i[-\frac{\omega A}{s}DK_1(A) + \omega K_1(|\omega|) - \omega|\omega|K_2(|\omega|)] \quad (31)$$

$$b_3 = \frac{\omega^2}{s}K_0(A) + \frac{A}{s}K_1(A) \quad (32)$$

$$b_4 = |\omega|[K_2(|\omega|) + K_0(|\omega|) + |\omega|K_1(|\omega|)] \quad (33)$$

$$b_5 = -i\omega[|\omega|K_0(|\omega|) + K_1(|\omega|)] \quad (34)$$

$$M = b_2 b_5 - b_1(Db_3 + b_4) \quad (35)$$

After the determination of all the coefficients, analytical solutions for the displacement, hoop stress, excess pore fluid pressure and fluid discharge are obtained through the numerical inversion method. Since the curves of displacement, stress, excess pore pressure and fluid discharge for Boundary condition I are similar to those for Boundary condition II, the similar jet-grouting responses will be represented and illustrated by the curves for Boundary condition II in this study.

Fig. 3 shows the variation of the radial displacement with the dimensionless loading length at the borehole wall ($z = 0$) under boundary condition II for different time during the jet-grouting process. The displacement is normalized with the shear modulus G and the limit grouting pressure f_u, which can reduce the parameters to only one, namely the exponent, B. As seen from the figure, the radial displacement grows fast when $\tilde{b}$ is small and gradually approaches an asymptotic value. It can also be seen that the radial displacement increases with the increase of grouting time, which can be well explained by the fact that the grouting pressure increases rapidly at first and remains nearly constant after τ reaches a certain value.

Fig. 4 displays the relationship between the hoop stress and the loading length at the cavity wall ($z = 0$). Note that the hoop stress can be directly normalized with the ultimate grouting pressure f_u. Consistent with the result from the research of Rajapakse (1993), the circumferential stress increases from an initially negative value, which indicates compressive stress, to a positive limit value for all time instants. Different from the solution presented by Rajapakse (1993), the maximum circumferential stress in this paper largely depends on grouting time and will not converge to the same asymptotic value, which increases with the increase of grouting time. This is because the grouting pressure in Rajapakse's study remains constant all the time, while the time-dependent grouting pressure here increases fast initially and approaches an asymptotic value quickly after grouting begins.

Fig. 5 plots the radial distribution of the excess pore fluid pressure ($z = 0$) for different grouting time and loading lengths. Also, the limit grouting pressure f_u is used to non-dimensionalized the excess pore fluid pressure. It can be clearly seen from the figure that the relationships between the excess pore fluid pressure and the radial distance are similar for different grouting times. The excess pore fluid pressure starts from zero and finally comes back to zero infinitely far away from the borehole wall. It should also be noted that the excess pore pressure decays to zero more rapidly with the radial distance for smaller τ. The two phenomena can be explained by the facts that the borehole wall is fully permeable and the soil at the same position undergoes more severe disturbance due to the squeezing effects with the permeation of grout. Another noteworthy point is that the increase in loading length will postpone the presence of the peak of the curve and result in an increase in

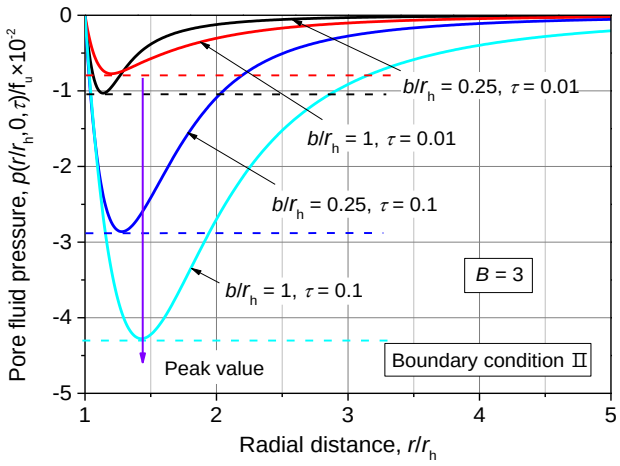

Fig. 5 Radial distribution of excess pore fluid pressure ($z = 0$) for different loading lengths and grouting time under boundary condition II

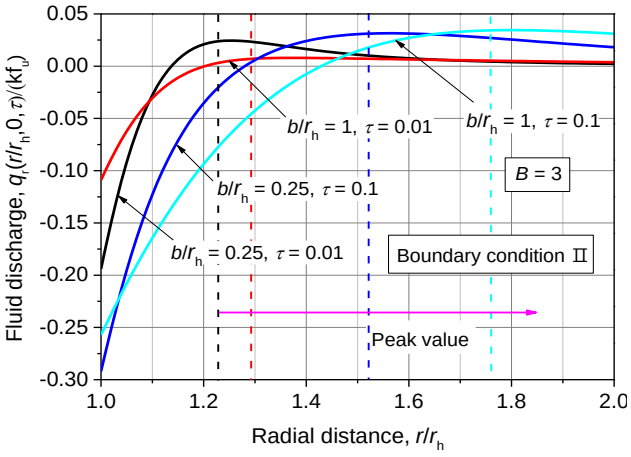

Fig. 6 Radial distribution of fluid discharge ($z = 0$) for different loading lengths and grouting time under boundary condition II

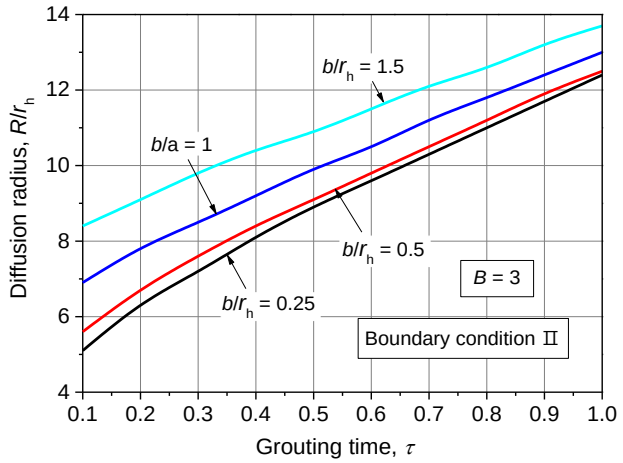

Fig. 7 Variation of diffusion radius of grouts with grouting time for different loading lengths under boundary condition II

the peak value, which indicates that the loading length shows significant impact on the maximum excess pore pressure.

Fig. 6 displays the radial distributions of fluid discharge in the porous medium ($z = 0$) for different grouting time and loading lengths. The discharge is normalized with the permeability coefficient k and the maximum grouting pressure f_u. As seen from the figure, the discharge is negative when the radial distance is small, which illustrates that the grout flow inward near the cavity wall. It is interesting to note that the radial discharge at the borehole wall increases with the decrease of the loading length, which indicates that changes in the loading length impose pronounced effect on the fluid discharge at the cavity wall. Further inspection of the figure reveals that the utmost discharge does not change significantly with loading length, which implies that the loading length has an insignificant effect on the maximum fluid discharge.

Fig. 7 plots the variation of the permeation radius of grout with grouting time for different loading lengths. It should be noted that the permeation radius can be obtained by seeking the radial position where the fluid discharge decreases to zero. This can be well illuminated by the fact that discharge of grout vanishes outside the reinforced region in the porous media. The permeation radius is easily normalized with the radius of the borehole r_h. It is clear that the permeation radius increases with the increase of $\tilde{b}$ and depends more significantly on the loading length when the loading length increases. This indicates that the grouting effect can be improved by increasing the length of the loading section. It is also interesting to note that the relationships between the permeation radius and grouting time are similar for different loading lengths, which means that the permeation rate of grout varies insignificantly when the dimensionless loading length changes.

4.2 Intermittent trigonometric grouting pressure-time relationship

Intermittent grouting is commonly encountered during the installation process of rotary grouting piles, and thus it is necessary to determine a periodic function for a proper description of this kind of grouting method. An intermittent trigonometric function is selected to model the grouting pressure-time relationship and the corresponding boundary condition for τ ranging from $2n\pi$ to $2(n+1)\pi$ is given by

$$\sigma_{rr}(1,\tilde{z},\tau) = -f_u \sin(\tau)\, H\big((2n+1)\pi - \tau\big)\big[\big(H(\tilde{z}+\tilde{b}) - H(\tilde{z}-\tilde{b})\big] \tag{36}$$

where f_u is the amplitude of the trigonometric function; n is a random positive integer.

Applying the Laplace-Fourier transform, Eq. (36) can be rewritten as

$$\sigma^*_{rr}(1,\omega,s) = -2\frac{1+e^{-2\pi}}{1-e^{-2\pi}}\frac{1}{1+s^2}\frac{\sin(\omega\tilde{b})}{\omega} \tag{37}$$

Thus, it is convenient to obtain the coefficients, C_1, C_3 and C_4, by substituting Eq. (37) for p_g^* in Eq. (24).

Fig. 8 plots the variation of permeation radius of grout with grouting time under boundary condition I. The dimensionless loading length $2\tilde{b}$ is taken as 0.5. It can be

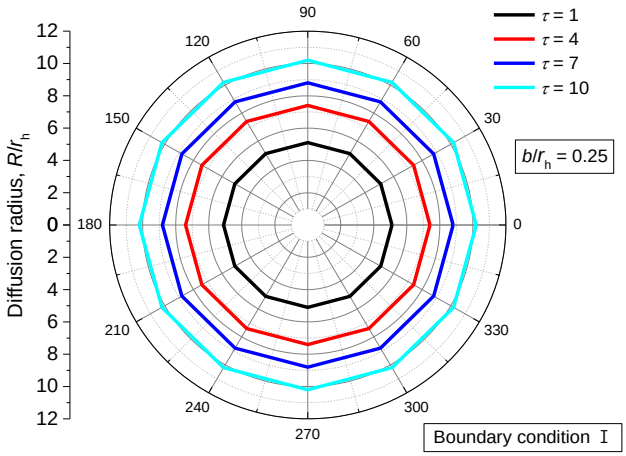

Fig. 8 Reinforced region of grouts for different grouting time under boundary condition I

clearly seen that the permeation radius initially grows rapidly, the rate of which gradually declines and tends to a constant value. This is because the soil becomes dense due to the squeezing effects induced by propagation of the grouting fluids.

4.3 Comparisons

Fig. 9 shows the reinforced regions under two kinds of grouting pressure when $\tau = 1$ and the dimensionless loading length is taken as 0.5 and 3, respectively. The exponent in the exponential grouting pressure-time relationship is equal to 3. It can be seen that the permeation radius of grout is larger under boundary condition II. This phenomenon can be explained by the fact that the grouting pressure increases more rapidly under the second boundary condition. It is also interesting to note that the permeation radius of grout increases with the increase of loading length, which is consistent with the result shown in Fig. 7.

Fig. 10 compares the radial displacement at the cavity wall ($z = 0$) for the two kinds of boundary conditions. It should be noted that the radial displacement under

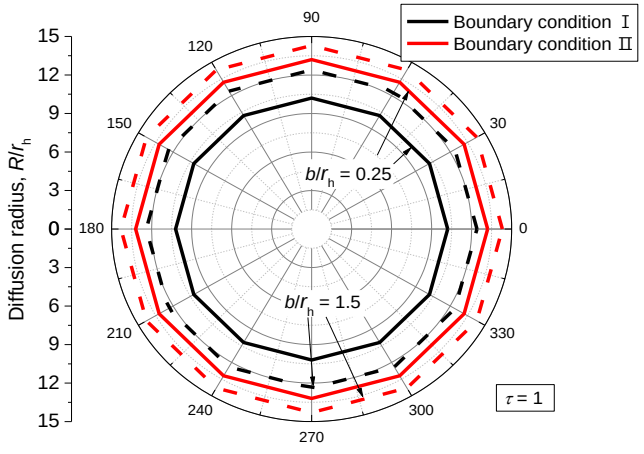

Fig. 9 Comparison of reinforced regions of grouts for different loading lengths under two boundary conditions

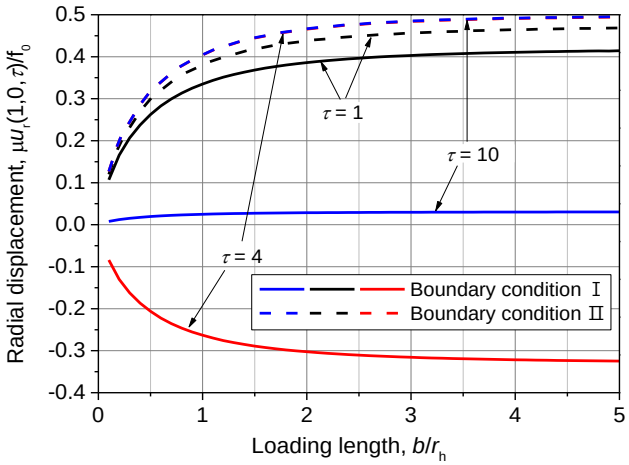

Fig. 10 Comparison of variations of radial displacement at borehole wall ($z = 0$) with loading length for different grouting time under two boundary conditions

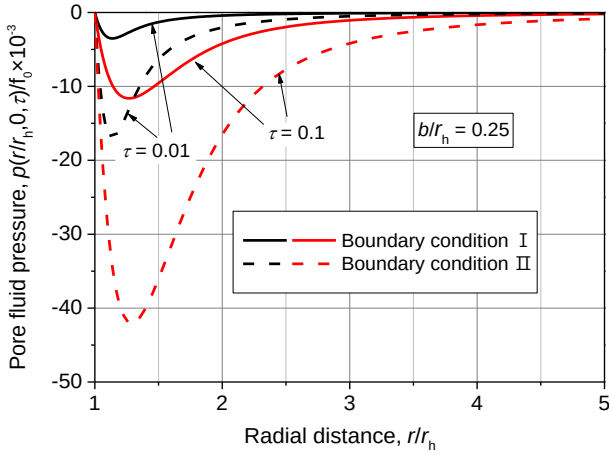

Fig. 11 Comparison of radial distributions of excess pore fluid pressure for different grouting time under two boundary conditions

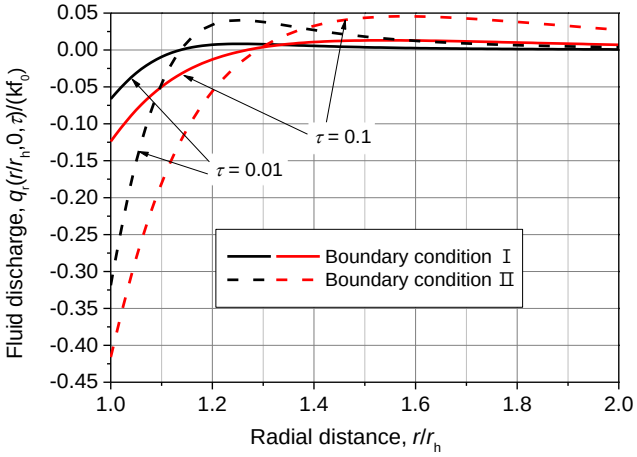

Fig. 12 Comparison of radial distributions of fluid discharge for different grouting time under two boundary conditions

intermittent grouting pressure is negative when $\tau = 4$. This can be well explained by the fact that the grouting pressure vanishes for some time in a period, which results in

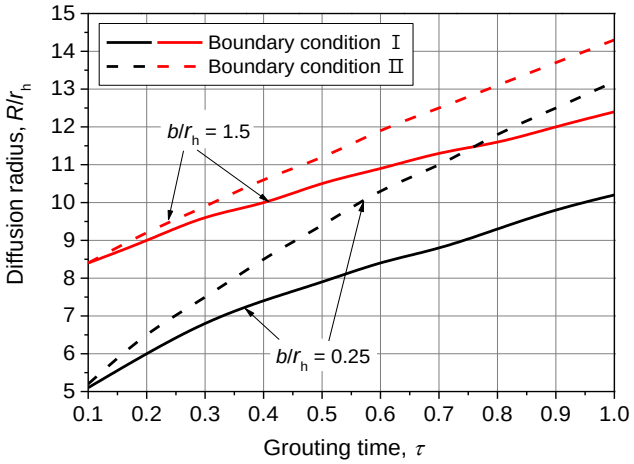

Fig. 13 Comparison of variations of diffusion radius of grouts with grouting time for different loading lengths under two boundary conditions

contraction of the borehole. It also can be clearly seen that for the second boundary condition, the radial displacements at the cavity wall when $\tau = 4$ and 10 are nearly the same. The observation can be illustrated with the reason that the grouting pressure approaches the asymptotic value quickly after grouting begins.

Fig. 11 displays the radial distributions of the excess pore fluid pressure ($z = 0$) for the two kinds of boundary conditions. The dimensionless loading length is taken as 0.5. As seen from the figure, the peak value of the distribution curve for exponential grouting pressure is much larger than that for intermittent grouting pressure. This indicates that the grouting pressure-time relationship has a pronounced effect on the maximum excess pore fluid pressure. Another noteworthy point is that the excess pore fluid pressure reaches the maximum value at the same radial position for boundary condition I and II.

Fig. 12 plots the radial distributions of fluid discharge for the two boundary conditions. As seen from the figure, the fluid discharge increases from a negative value to a positive maximum value and subsequently decreases to zero. This indicates that for different boundary conditions, the grouting fluids all flow inward near the cavity wall. It is also interesting to note that the peak value corresponding to boundary condition II is substantially larger than that under the first boundary condition. The phenomenon can be explained by the fact that the increasing rate of grouting pressure is higher for exponential grouting pressure-time relationship.

The grouting effect for each boundary condition is also investigated, as shown in Fig. 13. The dimensionless loading length $2\tilde{b}$ is taken as 0.5 and 3, respectively. It is easy to find that the permeation radii for the two boundary conditions are nearly the same immediately after the grouting fluids are injected into the soil. The permeation rate of grout for boundary condition II then significantly exceeds that for boundary condition I, which demonstrates that the grouting pressure increases faster for the second boundary condition. This indicates that the grouting effect can be greatly improved by altering the grouting pressure-time relationship.

5. Parametric study

In this section, parametric study is conducted on boundary condition II to investigate the effect of model parameter on the solutions. It should be noted that the presented results are all normalized with some properties of the porous medium or model parameters, such as the shear modulus G, the permeability coefficient of soil k and the limit grouting pressure f_u. Therefore, the parameter that still needs to be analyzed denotes the exponent in boundary condition II, which is referred to as B. The exponent B stands for the increasing rate of the grouting pressure from zero to the limit value, and thus the results of the parametric study may be used to control grouting pressure during the jet-grouting process of ground improvement when similar boundary conditions are applied.

Fig. 14 displays the variation of radial displacement at the cavity wall ($z = 0$) with the exponent for different loading lengths when $\tau = 1$. As seen from the figure, the radial displacement increases with the increase of B. This phenomenon is for the reason that the grouting pressure grows more rapidly with time for larger B. It can also be found that the impact of B decays as B increases. The observation can be well explained by the fact that the

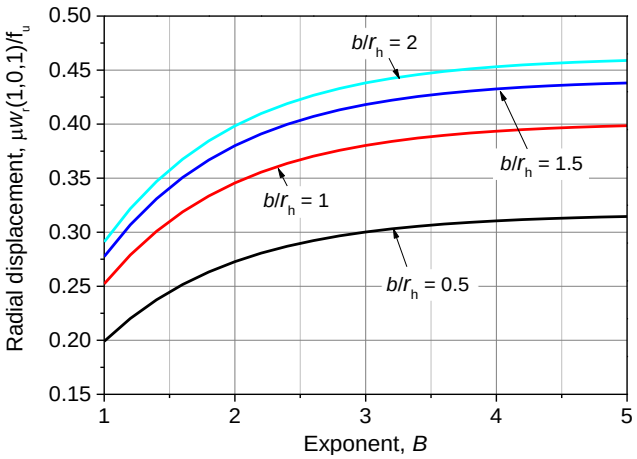

Fig. 14 Variation of radial displacement at borehole wall ($z = 0$) with B for different loading lengths

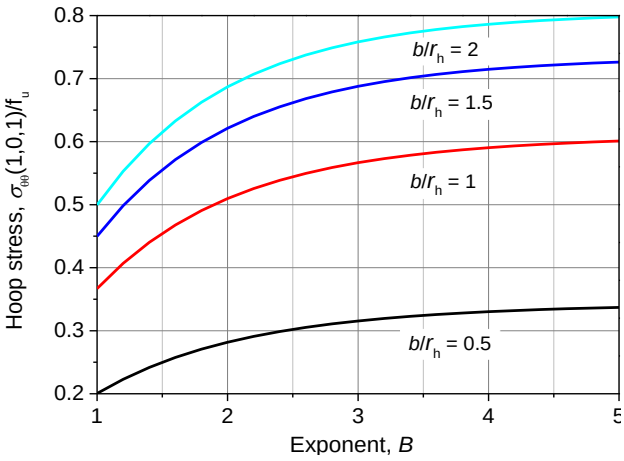

Fig. 15 Variation of hoop stress at borehole wall ($z = 0$) with B for different loading lengths

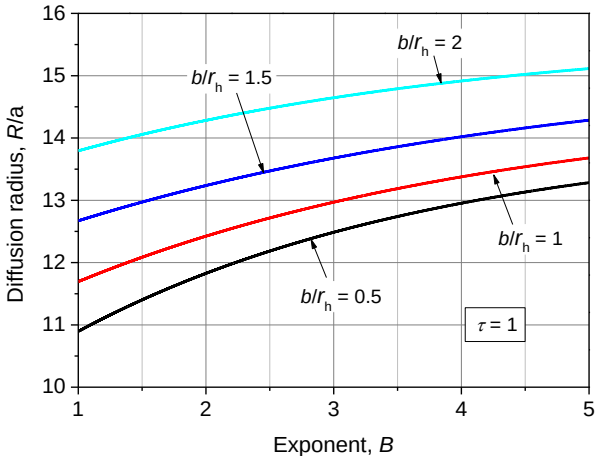

Fig. 16 Variation of diffusion radius of grouts with B for different loading lengths

increasing rate of grouting pressure changes insignificantly when $B > 3$.

The variation of the hoop stress at the cavity wall ($z = 0$) with the exponent when $\tau = 1$ is shown in Fig. 15. The dimensionless loading length is taken as 0.5, 1, 1.5 and 2. It can be seen from the figure that the hoop stress also increases with the increase of B when $B < 3$ and approaches a limit value thereafter, which can be illustrated with the same reason as that in analysis of Fig. 14. Further inspection of the figure reveals that the hoop stress increases more rapidly with the exponent as the loading length increases. This indicates that the impact of B on the hoop stress changes with the variation of the loading length.

Fig. 16 plots the variation of the permeation radius of grout with the exponent for different loading lengths. It is clear that the permeation radius increases with the increase of B, which implies that the grouting effect can be improved by increasing the growing rate of the grouting pressure. It should also be noted that the effect of B on the permeation radius decays as the loading length increases. This indicates that the loading length slightly influences the impact of the exponent on the grouting effect.

6. Conclusions

In this paper, the poroelastic solutions, coupling soil deformation and permeation of grout, are developed based on Biot's poroelasticity theory to model the grouting effects during the jet-grouting process. Two kinds of boundary conditions, with respect to the grouting pressure, are selected to simulate the grouting process in ground improvement and rotary grouting pile installation. Different from the constant uniform radial traction applied to the borehole wall in Rajapakse's study (1993), the grouting pressure in this study, which varies with time during the jet-grouting process, is determined according to the actual grouting technique in ground improvement and rotary grouting pile installation. The advantage of adopting such time-dependent boundary conditions is that the grouting process in practical engineering can be modeled more realistically. The grouting pressure-time relationships are described with the intermittent trigonometric function and the exponential function, for jet-grouting in ground improvement and rotary grouting pile installation.

The results reveal that the excess pore fluid pressure increases with the increase of grouting time immediately after grouting fluids are injected into the soil as the grouting pressure increases with time initially. The fluid discharge is negative near the cavity wall and becomes positive when the radial distance reaches a certain value, which indicates that the fluid flow is inward near the borehole wall. Results from parametric study imply that the radial displacement at the cavity wall ($z = 0$) increases with the increase of B. This phenomenon can be explained with the reason that larger B results in higher increasing rate of the grouting pressure. As for the grouting effect, the exponent B turns out to show a pronounced effect on the permeation radius, which also increases with the increase of B. The current study provides a feasible analytical tool for estimating the permeation radius of grouts so as to assess the jet-grouting effects in ground improvement and rotary grouting pile installation in soft clayey soils. However, it should be noted that since the jet-grouting mechanism in coarse gravel is governed by the seepage of the injected grouts, the proposed model developed for clayey soil is not applicable for jet-grouting problems in coarse gravel.

Acknowledgments

The research described in this paper was financially supported by the National Natural Science Foundation of China (Grant No. 41772290).

References

Abousleiman, Y. and Cui, L. (1998), "Poroelastic solutions in transversely isotropic media for wellbore and cylinder", *Int. J. Solids Struct.*, **35**(34-35), 4905-4929. https://doi.org/10.1016/S0020-7683(98)00101-2.

Bergado, D.T., Anderson, L.R., Miura, N. and Balasubramaniam, A.S. (1996), *Soft Ground Improvement in Lowland and Other Environments*, ASCE.

Biot, M.A. (1941), "General theory of three-dimensional consolidation", *J. Appl. Phys.*, **12**(2), 155-164. https://doi.org/10.1063/1.1712886.

Cai, Y., Shi, B., Ng, C.W. and Tang, C.S. (2006), "Effect of polypropylene fibre and lime admixture on engineering properties of clayey soil", *Eng. Geol.*, **87**(3-4), 230-240. https://doi.org/10.1016/j.enggeo.2006.07.007.

Celik, F. (2019), "The observation of permeation grouting method as soil improvement technique with different grout flow models", *Geomech. Eng.*, **17**(4), 367-374. https://doi.org/10.12989/gae.2019.17.4.367.

Chang, M.H., Mao, T.W. and Huang, R.C. (2016), "A study on the improvements of geotechnical properties of in-situ soils by grouting", *Geomech. Eng.*, **10**(4), 527-546. https://doi.org/10.12989/gae.2016.10.4.527.

Detournay, E. and Cheng, A.D. (1988), "Poroelastic response of a borehole in a non-hydrostatic stress field", *Int. J. Rock Mech. Min. Sci. Geomech. Abstr.*, **25**(3), 171-182. https://doi.org/10.1016/0148-9062(88)92299-1.

Hassler, L., Hakansson, U. and Stille, H. (1992). "Computer-

simulated flow of grouts in jointed rock", *Tunn. Undergr. Sp. Technol.*, **7**(4), 441-446. https://doi.org/10.1016/0886-7798(92)90074-R.

Hou, F., Sun, K., Wu, Q., Xu, W. and Ren, S. (2019), "Grout diffusion model in porous media considering the variation in viscosity with time", *Adv. Mech. Eng.*, **11**(1), 1687814018819890. https://doi.org/10.1177%2F1687814018819890.

Jalili, M., Zare, A. and Shabani, M.J. (2019), "Parametric and numerical study on soft ground improvement using stone column reinforced with geogrid", *J. Eng. Geol.*, **12**(4), 571-598.

Kim, D. and Park, K. (2017), "Evaluation of the grouting in the sandy ground using bio injection material", *Geomech. Eng.*, **12**(5), 739-752. https://doi.org/10.12989/gae.2017.12.5.739.

Li, L., Xiang, Z.C., Zou, J.F., and Wang, F. (2019), "An improved model of compaction grouting considering three-dimensional shearing failure and its engineering application", *Geomech. Eng.*, **19**(3), 217-227. https://doi.org/10.12989/gae.2019.19.3.217.

Lignola, G.P., Flora, A. and Manfredi, G. (2008), "Simple method for the design of jet grouted umbrellas in tunneling", *J. Geotech. Geoenviron. Eng.*, **134**(12), 1778-1790. https://doi.org/10.1061/(ASCE)1090-0241(2008)134:12(1778).

Liu, H., Zhou, H., Kong, G., Qin, H. and Zha, Y. (2017), "High pressure jet grouting column installation effect in soft soil: Theoretical model and field application", *Comput. Geotech.*, **88**, 74-94. https://doi.org/10.1016/j.compgeo.2017.03.005.

Mehrabian, A. and Abousleiman, Y.N. (2013), "Generalized poroelastic wellbore problem", *Int. J. Numer. Anal. Meth. Geomech.*, **37**(16), 2727-2754. https://doi.org/10.1002/nag.2160.

Modoni, G., Croce, P. and Mongiovi, L. (2006), "Theoretical modelling of jet grouting", *Géotechnique*, **56**(5), 335-348. https://doi.org/10.1680/geot.2006.56.5.335.

Njock, P.G.A., Shen, J.S., Modoni, G. and Arulrajah, A. (2018), "Recent advances in horizontal jet grouting (HJG): An overview", *Arab. J. Sci. Eng.*, **43**(4), 1543-1560.

Rajapakse, R.K.N.D. (1993), "Stress analysis of borehole in poroelastic medium", *J. Eng. Mech.*, **119**(6), 1205-1227. https://doi.org/10.1061/(ASCE)0733-9399(1993)119:6(1205).

Shehata, H. and Poulos, H. (2018), "Latest thoughts on ground improvement techniques", *Proceedings of the 2nd GeoMEast International Congress and Exhibition on Sustainable Civil Infrastructures*, Giza, Egypt, November.

Shen, S.L., Wang, Z.F. and Cheng, W.C. (2017), "Estimation of lateral displacement induced by jet grouting in clayey soils", *Géotechnique*, **67**(7), 621-630. https://doi.org/10.1680/jgeot.16.P.159.

Singh, S. (2018), "A review on trends in ground improvement techniques", *J. Geotech. Eng.*, **5**(1), 18-22.

Song, Z., Liang, F., Lin, C. and Xiang, Y. (2019), "Interaction of pore pressures in double-porosity medium: Fluid injection in borehole", *Comput. Geotech.*, **107**, 142-149. https://doi.org/10.1016/j.compgeo.2018.11.026.

Stehfest, H. (1970), "Algorithm 368: Numerical inversion of Laplace transforms", *Commun. ACM*, **13**(1), 47-49. https://doi.org/10.1145/361953.361969.

Sun, Y., Zhang, J., Li, G., Ma, G., Huang, Y., Sun, J., Wang, Y. and Nener, B. (2019), "Determination of Young's modulus of jet grouted coalcretes using an intelligent model", *Eng. Geol.*, **252**, 43-53. https://doi.org/10.1016/j.enggeo.2019.02.021.

Wallner, M. (1976), "Propagation of sedimentation stable cement pastes in jointed rock", *Rock Mech. Waterways Constr.*, **2**, 132-136.

Yang, X.Z., Wang, X.H. and Lei, J.S. (2004), "Study on grouting diffusion radius of Bingham fluids", *J. Hydraul. Eng.*, **6**, 75-79.

Yang, Z.Q., Hou, K.P., Guo, T.T. and Qiu, M.A. (2011), "Study of column-hemispherical penetration grouting mechanism based on Bingham fluid of time-dependent behavior of viscosity", *Rock Soil Mech.*, **32**(9), 2697-2703.

Zhang, N., Li, Z., Ma, Q., Ma, T., Niu, X., Liu, X. and Feng, T. (2018), "SI model of horizontal jet grouting reinforcement for soft soil", *Geomech. Eng.*, **15**(5), 1029-1038. https://doi.org/10.12989/gae.2018.15.5.1029.

Zhang, N., Shen, S.L., Wu, H.N., Chai, J.C., Xu, Y.S. and Yin, Z.Y. (2015), "Evaluation of effect of basal geotextile reinforcement under embankment loading on soft marine deposits", *Geotext. Geomembr.*, **43**(6), 506-514. https://doi.org/10.1016/j.geotexmem.2015.05.005.

Zou, J.F, and Zuo, S.Q. (2017). Similarity solution for the synchronous grouting of shield tunnel under the vertical non-axisymmetric displacement boundary condition. *Adv. Appl. Math. Mech.*, **9**(1), 205-232. https://doi.org/10.4208/aamm.2016.m1479.

Zou, J.F. and Zhang, P.H. (2019), "Analytical model of fully grouted bolts in pull-out tests and in situ rock masses", *Int. J. Rock Mech. Min. Sci.*, **113**, 278-294. https://doi.org/10.1016/j.ijrmms.2018.11.015.

JS